

# Evidence for Neutrino Flux Variability and its Implications

D.O. Caldwell

*Physics Department, University of California, Santa Barbara, CA 93106-9530, USA*

P.A. Sturrock

*Center for Space Science and Astrophysics, Stanford University, Stanford, CA 94305-4060, USA*

(Dated: April 15, 2019)

While KamLAND apparently rules out Resonant-Spin-Flavor-Precession (RSFP) as an explanation of the solar neutrino deficit, the solar neutrino fluxes in the Cl and Ga experiments appear to vary with solar rotation. Added to this evidence, summarized here, a power spectrum analysis of the Super-Kamiokande data reveals significant variation in the flux matching a dominant rotation rate observed in the solar magnetic field in the same time period. Three frequency peaks, all related to this rotation rate, can be explained quantitatively. A Super-Kamiokande paper reported no time variation of the flux, but showed the same peaks as statistically insignificant, resulting from an inappropriate analysis. This modulation would be small (7%) in the Super-Kamiokande energy region (and below the sensitivity of the Super-Kamiokande analysis) for RSFP as a subdominant neutrino process in the convection zone. Especially the radiochemical data display effects that correspond to solar-cycle changes in the magnetic field, typical of the convection zone. This subdominant process requires new physics: a large neutrino transition magnetic moment and a light sterile neutrino. It does, however, fix current problems in providing fits to all experimental estimates of the mean neutrino flux, and is compatible with the extensive evidence for solar neutrino flux variability.

PACS numbers: 26.65.+t, 14.60.Pq, 14.60.St

## INTRODUCTION

Results from the KamLAND experiment [1] seem to confirm the Large-Mixing Angle (LMA) solution to the solar neutrino deficit and rule out the Resonant-Spin-Flavor-Precession (RSFP) explanation [2]. On the other hand, there is increasing evidence [3, 4, 5, 6, 7, 8, 9] that the solar neutrino flux is not constant as assumed for the LMA solution, but varies with well-known solar rotation periods. The solar neutrino situation may be more complex than usually assumed, and RSFP could be subdominant to LMA [10], requiring both a large transition magnetic moment and a light sterile neutrino. Since this recent information on solar neutrino variability is not widely known, a brief summary is presented here of analyses of radiochemical neutrino data, along with newer input from the Super-Kamiokande experiment [11]. While the 10-day averages of Super-Kamiokande solar neutrino data [12] show no obvious time dependence, power-spectrum analyses [13] displayed a strong peak at the frequency  $26.57 \pm 0.05 \text{ y}^{-1}$  (period 13.75 d), as well as one at  $9.42 \text{ y}^{-1}$ . However, a subsequent Super-Kamiokande paper [14] provided 5-day averages of the data, and there was no longer evidence for the  $26.57 \text{ y}^{-1}$  peak, showing it to be an alias of the  $9.42 \text{ y}^{-1}$  peak (which will be explained later) due to the extremely regular 10-day binning. In the 5-day data the  $9.42 \text{ y}^{-1}$  is enhanced. We also find a peak at  $39.28 \text{ y}^{-1}$ , which is the frequency of a dominant rotation-related oscillation in the photospheric magnetic field. Another notable peak at  $43.72 \text{ y}^{-1}$  may be attributed to the same physical process responsible for the peak at  $9.42 \text{ y}^{-1}$ .

The suggested subdominant process providing these peaks arises from an RSFP transition in which the solar  $\nu_e$  changes to a different flavor, and the spin is flipped. As in the MSW process [15], this can occur resonantly at an appropriate solar density. The two processes, LMA MSW and RSFP, would appear sequentially at very different solar radii. The LMA transition would occur at a relatively small solar radius, since the resonant mass-squared difference is  $\sim 10^{-4} \text{ eV}^2$ , while the RSFP resonance would be at a much larger radius corresponding to a difference of  $\Delta m^2 \sim 10^{-8} \text{ eV}^2$ . The two quite different  $\Delta m^2$  values require that there be another mass state, and the width of the  $Z^0$  boson necessitates that the associated flavor state be sterile. A sterile state was also suggested by de Holanda and Smirnov [16], since such a subdominant transition would improve agreement with the Homestake data [17] and the Super-Kamiokande energy dependence [11]. In the RSFP case, the small sterile neutrino mixing is replaced by a magnetic moment transition, and again a decided improvement in the fit to the solar neutrino data is obtained [10]. This improvement, and also the reason RSFP by itself actually provides a better fit to mean solar data than does LMA [18, 19], results from the shape of the RSFP neutrino survival probability. It has a resonance pit at a density that suppresses the 0.86 MeV  ${}^7\text{Be}$  line (as does the Small-Mixing Angle [SMA] solution), but tends toward 1/2 and hence fits the Super-Kamiokande spectrum, whereas the survival probability goes to unity in the SMA case. The high-energy rise includes the neutral current scattering of the products of the spin-flavor flips, which need to be active, and hence Majorana neutrinos are required in order to fit [19] the

SNO data [20] for RSFP by itself. In the case of subdominant RSFP, the high-energy behavior is determined mainly by the MSW transition, since the observed flux modulation is small ( $\sim 7\%$ ) in the  $^8\text{B}$  neutrino region. Going down to intermediate energies, the dip toward the resonance pit reduces the predicted rate for the Homestake experiment [17], improving agreement with data, and eliminates the rise below  $\sim 8$  MeV which is predicted by the LMA solution but not observed by Super-Kamiokande [11] or SNO [20]. The electron-neutrino-associated sterile neutrino, which provides a better fit to the solar data and is required for subdominant RSFP, is different from the muon-neutrino-associated sterile neutrino needed for the results of the LSND experiment [21]. Possibly three sterile neutrinos exist with a family symmetry.

## REVIEW OF PAST EVIDENCE

The RSFP framework provides a convenient way to understand the data, and hence it will be used here, initially to aid in a brief review of the published evidence for solar neutrino flux variability. By analyzing  $10^3$  simulated data sequences, it was found [3] that the variance of the Homestake solar neutrino data [17] is larger than expected at the 99.9% confidence level (CL). A power spectrum analysis [3] of the data showed a peak at  $12.88 \pm 0.02 \text{ y}^{-1}$  (28.4 d), compatible with the rotation rate of the solar radiative zone. Peak widths are computed for a probability drop to 10%. Four sidebands to the  $12.88 \text{ y}^{-1}$  frequency gave evidence at the 99.8% CL for a latitudinal effect associated with the tilt of the sun's rotation axis, and the latitude dependence was also seen directly in the data at the 98% CL [4].

The GALLEX data [22] showed a peak at  $13.59 \pm 0.04 \text{ y}^{-1}$ , compatible with the equatorial rotation rate of the deep convection zone. This peak is also in the Homestake data, and a combined analysis of both data sets shows that the  $13.59 \text{ y}^{-1}$  peak is larger than in either data set alone. Comparison [7] of the power spectrum for the GALLEX data with a probability distribution function for the solar synodic rotation frequency as a function of radius and latitude, derived from SOHO/MDI helioseismology data [23], results in Fig. 1. This map shows that the rotation frequency matches the neutrino modulation in the equatorial section of the convection zone at about 0.8 of the solar radius,  $R_{\odot}$ .

The influence of these rotation frequencies extends even to the corona, since the SXT instrument [24] on the Yohkoh spacecraft provides X-ray evidence for two ‘‘rigid’’ rotation rates, one ( $13.55 \pm 0.02 \text{ y}^{-1}$ ) mainly at the equator, and the other ( $12.86 \pm 0.02 \text{ y}^{-1}$ ) mainly at high latitudes. These values are in remarkable agreement [8] with the neutrino modulation frequencies and also with their equatorial location in one case and non-

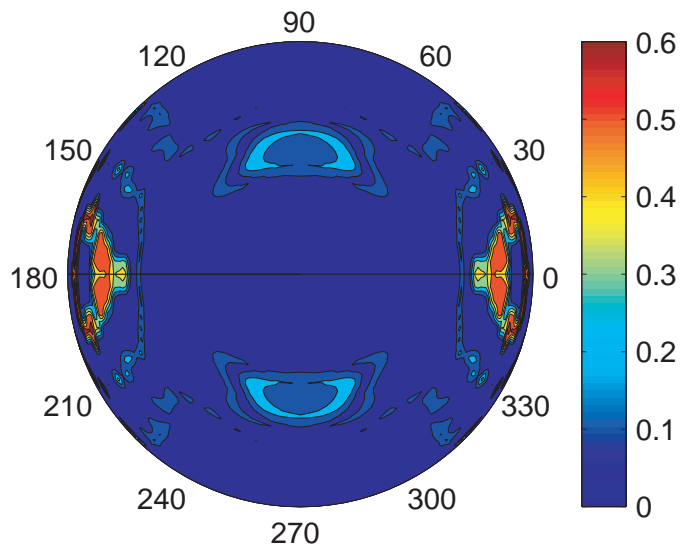


FIG. 1: Map of the resonance statistic of the SOHO/MDI helioseismology and GALLEX data on a meridional section of the solar interior. The only high probability areas (red) are lens-shaped sections near the equator, and all others are low probability.

equatorial in the other; see Fig. 2. A plausible interpretation of this result is that a large-scale magnetic structure deep in the convection zone modulates the neutrino flux and is also responsible for the structure of the low- $k$  component of the photospheric magnetic field (where  $k$  is wave-number), and that the coronal magnetic field reflects the low- $k$  components rather than the high- $k$  components that arise from granulation.

The fact that coronal X-rays and the neutrino flux both show evidence of two dominant rotation frequencies is quite consistent with similar results of the analyses of other solar variables. For instance, an analysis [25] of the photospheric magnetic field during solar cycle 21 found two dominant magnetic regions: one in the northern hemisphere with synodic rotation frequency  $\sim 13.6 \text{ y}^{-1}$ , and the other in the southern hemisphere with synodic rotation frequency  $\sim 13.0 \text{ y}^{-1}$ . Similarly, an analysis [26] of flares during solar cycle 23 found a dominant synodic frequency of  $\sim 13.5 \text{ y}^{-1}$  for the northern hemisphere and  $\sim 12.9 \text{ y}^{-1}$  for the southern hemisphere. These and other studies show a strong tendency for magnetic structures to rotate either at about  $12.9 \text{ y}^{-1}$  or at about  $13.6 \text{ y}^{-1}$ . Since the Sun's magnetic field is believed to originate in a dynamo process at or near the tachocline, it is possible that some magnetic flux is anchored in the radiative zone just below the tachocline, where the synodic rotation frequency is about  $12.9 \text{ y}^{-1}$ , and some just above the tachocline in the convection zone, where the synodic rotation frequency is about  $13.6 \text{ y}^{-1}$ . It is also possible that the  $12.9 \text{ y}^{-1}$  frequency results from a latitudinal wave motion in the convection zone excited by

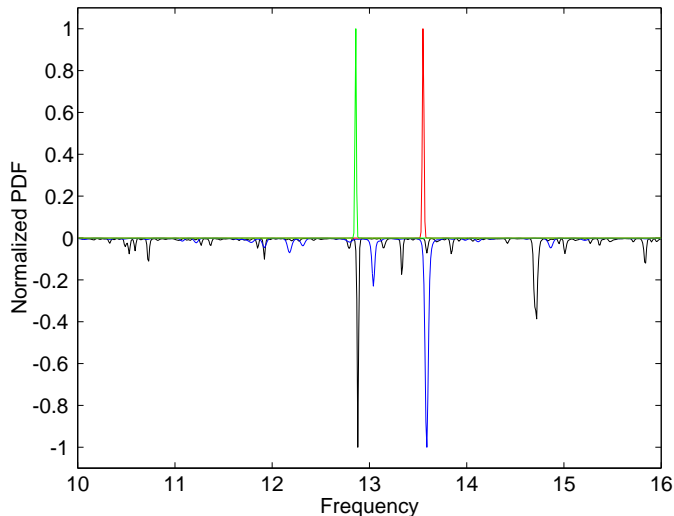


FIG. 2: Comparison of normalized probability distribution functions formed from power spectra of data from SXT equator (red), SXT N60-S60 (green), Homestake (black), and GALLEX (blue). Note that the SXT (red) and GALLEX data are equatorial, and the other two are not. In this and all subsequent figures frequencies are in cycles per year.

structures at or near the tachocline.

An example of latitudinal oscillatory motion of magnetic structures may be the well-known Rieger-type oscillations (seen in gamma-ray flares, sunspots, etc.) with frequencies of about 2.4, 4.7, and  $7.1 \text{ y}^{-1}$  [27, 29]. These periodicities may be attributed to r-mode oscillations [29] with spherical harmonic indices  $\ell = 3$ ,  $m = 1, 2, 3$ , giving frequencies  $\nu = 2m\nu_R/\ell(\ell + 1)$ , where  $\nu_R$  is the sidereal rotation rate [ $\nu(\text{sid}) = \nu(\text{syn}) + 1$ ]. These frequencies are also seen in neutrino data [3, 5, 9]. A joint spectrum analysis [9] of Homestake and GALLEX-GNO data yields peaks at 12.88, 2.33, 4.62, and  $6.94 \text{ y}^{-1}$ , indicating a sidereal rotation frequency  $\nu_R = 13.88 \pm 0.03 \text{ y}^{-1}$ . These r-mode frequencies provide further, and somewhat unexpected, evidence for neutrino flux variations, and we return later to another observation of them.

## OBSERVATIONS IN THE NEUTRINO CONTEXT

The difference between the main modulations detected by the Cl and Ga experiments may be explained by the tilt of the solar axis relative to the ecliptic, along with the fact that Cl and Ga neutrinos are produced mainly at quite different radii. The Ga data comes mostly—especially as the fit requires suppressing the  ${}^7\text{Be}$  line—from  $pp$  neutrinos, which originate predominantly at large solar radius ( $\sim 0.2 R_\odot$ ), so that the wide beam of neutrinos detected on earth is insensitive to axis tilt. Thus the beam of neutrinos detected by the Ga experiments exhibits no seasonal variation and can be mod-

ulated by the equatorial structure indicated in Fig. 1, leading to the observed frequency at about  $13.6 \text{ y}^{-1}$ . On the other hand, the Homestake experiment detects neutrinos produced from a smaller sphere ( $\sim 0.05 R_\odot$ ), so that the axis tilt causes these neutrinos mainly to miss the equatorial structure of Fig. 1 and instead sample nonzero latitudes where the  $12.9 \text{ y}^{-1}$  modulation may be more significant. Twice a year, axis tilt has no effect for these neutrinos, leading to a seasonal variation in the measured flux [4].

The  $13.6 \text{ y}^{-1}$  frequency, located as in Fig. 1, represents a modulation of the  $pp$  neutrinos which are at or near the steeply falling edge of the neutrino survival probability as it dips toward the RSFP resonance pit. This pit, which suppresses the  ${}^7\text{Be}$  neutrinos, is where the largest value of the mass-squared difference between the initial and final states, divided by their energy, satisfies

$$\Delta m^2/E = 2\sqrt{2}G_F N_{\text{eff}}, \quad (1)$$

and is essentially the same as for an MSW resonance [15], since it also arises from a difference in forward-scattering amplitudes of the two states. Ignoring angle factors, for MSW  $N_{\text{eff}} = N_e$  (the electron density), and for RSFP and active-active transitions,  $N_{\text{eff}} = N_e - N_n$  for Majorana neutrinos, where  $N_n$  is the neutron density (about  $N_e/6$  in the region of interest in the Sun). For Dirac neutrinos  $N_{\text{eff}} = N_e - N_n/2$ , but for RSFP alone (not the subdominant case), only Majorana neutrinos fit all the solar data. For the more complicated subdominant case involving a transition magnetic moment process to a sterile state, the numerical result of Ref. [10] may be used. It shows the resonant transition occurring close to  $0.8 R_\odot$  for  $\Delta m^2 = 1.8 \times 10^{-8} \text{ eV}^2$ , which provides a good fit to the data. This result is in remarkable agreement with the position shown in Fig. 1.

## CHANGES WITH SOLAR CYCLE

It is well known that the convection zone magnetic field changes with the solar cycle, so the neutrino modulation features described above should not be permanent. It has been argued [30] that an RSFP effect would have to be in the radiative zone, where the field does not change with the solar cycle, on the assumption that solar cycle variations are not manifested. On the contrary, we show here that solar cycle changes play an important role. Variations in neutrino rates are difficult to observe, since changes in field magnitude would be undetectable if the transition remains adiabatic, and even if flux modulation results, average rates may vary only slightly. The feature that is most sensitive to field magnitude or radial variations is the intersection of the very steeply falling  $pp$  neutrino spectrum with the edge of the RSFP resonance pit. The shape of the neutrino transition probability depends not only on the resonance location, Eq. (1), but also on

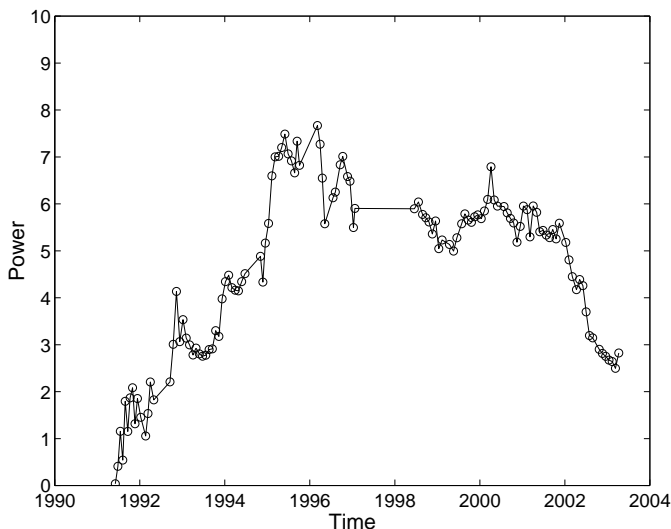


FIG. 3: Running Rayleigh power, as a function of end time, for frequency  $13.59 \text{ y}^{-1}$  from the GALLEX-GNO data. Note that the power builds up from the start of data taking after the 1990 solar maximum until the 1996.8 solar minimum, after which there is little evidence for that frequency.

the product of the magnetic moment and magnetic field. Thus a change in field will shift the intersection of the  $pp$  spectrum and resonant pit edge and change the degree of modulation. As can be seen in Fig. 3, the peak at  $13.6 \text{ y}^{-1}$  associated with these neutrinos increased in strength from the start of data taking after the solar maximum of 1989.6 to the solar minimum of 1996.8, after which the modulation becomes weak. Also it was during that cycle that the main buildup in the strength of the  $12.9 \text{ y}^{-1}$  oscillation was detected by Homestake. The SXT X-ray data, with which these two frequencies had remarkable agreement [8], also came from that same solar cycle.

Because of a paper [31] suggesting that the  $13.59 \text{ y}^{-1}$  line is not statistically significant in the GALLEX-GNO data, we recently showed [32] that this resulted from choices made in the analysis procedures. Using the most sensitive analysis choices, we found the  $13.59 \text{ y}^{-1}$  modulation is significant at the 99.9% confidence level.

Another feature attributable to a time variation of the intersection of the  $pp$  spectrum with the edge of the RSFP resonance pit is the appearance [6] of a bimodal flux distribution in the Ga data, as shown in Fig. 4. A single peak would be expected if there were no flux modulation. This structure is clearly evident during the same solar maximum to solar minimum period when the flux is binned appropriately using individual runs, instead of averaged over several data runs. This neutrino flux effect also diminishes after the solar minimum. Adding to the significance of this result is the plot of Fig. 5, which shows that when the end times of runs are reordered according to the phase of the  $13.59 \text{ y}^{-1}$  rotation, the flux values are low in one-half of the cycle and high in the other.

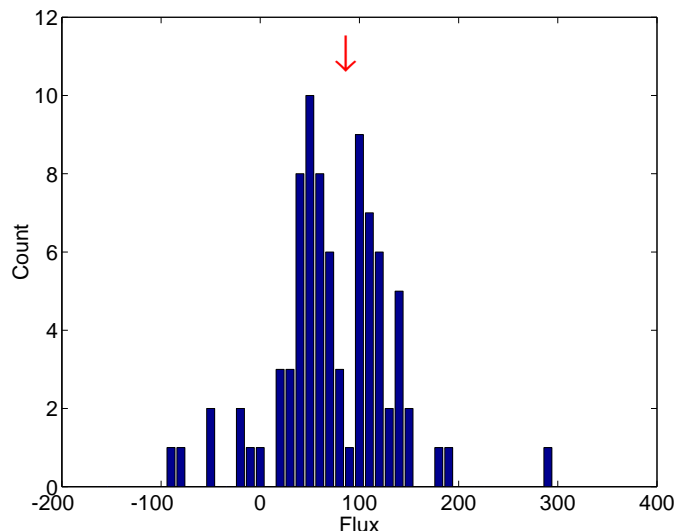


FIG. 4: Histogram of GALLEX data. The arrow indicates the maximum-likelihood estimate of the flux (in SNU).

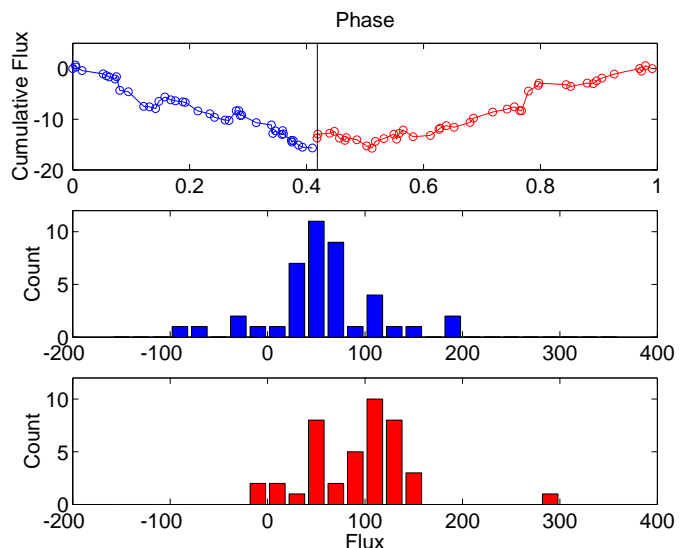


FIG. 5: Normalized GALLEX flux (in SNU) measurement runs (prior to 1997) reordered according to the phase of the  $13.59 \text{ y}^{-1}$  solar modulation. The division in phase is made so as to have equal numbers of events in the descending (blue) and ascending (red) parts of the cycle.

It is unfortunate that the Homestake experiment, which detected mainly the  $^8\text{B}$  neutrinos (the only neutrino component registered by Super-Kamiokande) ceased operation before Super-Kamiokande started. As a result, there is no way to predict from other solar neutrino experiments what neutrino flux variation should have been detected by Super-Kamiokande during its operation from May 1996 (near solar minimum) until July 2001 (near solar maximum). However, it is possible to compare Super-Kamiokande measurements with other

solar variables that reflect the influence of the Sun’s internal magnetic field.

### SUPER-KAMIOKANDE DATA ANALYSIS

The Super-Kamiokande group released [12] flux measurements in 184 bins of about 10 days each. The flux measurements vary over the range 2 : 1, and the fractional error of the measurement (averaged over all bins) is 0.14. Because of the regularity of the binning, the “window spectrum” (the power spectrum of the acquisition times) has a huge peak (power  $S > 120$ ) at a frequency of  $\nu = 35.98 \text{ y}^{-1}$  (period 10.15 d). (Note that the probability of obtaining a power of strength  $S$  or more by chance at a specified frequency [33] is  $e^{-S}$ .) This regularity in binning inevitably leads to severe aliasing of the power spectrum of the flux measurements, producing consequences explored below.

Analysis of the data in 10-day bins by a likelihood procedure outlined in the Appendix, in which the start and stop times for each bin were used so as to take into account the time over which data were taken, gave [13] the strongest peak in the range 0 to  $100 \text{ y}^{-1}$  at  $\nu = 26.57 \text{ y}^{-1}$  with  $S = 11.26$ , and the next strongest peak at  $\nu = 9.42 \text{ y}^{-1}$  with  $S = 7.29$ . Milsztajn, and subsequently the Super-Kamiokande group, used the Lomb-Scargle analysis method [33], which assigns data acquisition to discrete times (in this case chosen to be the mid-time of each bin) rather than to extended intervals. This “delta-function” form for the time window function is inappropriate, since the length of each bin is comparable with the periods of some of the oscillations of interest. It is also significant that the likelihood method takes measurement errors into account, whereas the Lomb-Scargle method as they used it does not. The Lomb-Scargle analysis by the Super-Kamiokande group [13] gave  $S = 10.7$  at  $\nu = 26.55 \text{ y}^{-1}$ , which was stated to correspond to 98.6% CL, while the ignored peak at  $9.41 \text{ y}^{-1}$  had  $S = 6.3$ . Subsequently, the Super-Kamiokande group modified their analysis to take account of the non-uniformity of data collection, assigning the flux and error measurements for each bin to a “mean live time” rather than the mid-time. This has resulted in a reduction to  $S = 7.51$  of the power at  $26.55 \text{ y}^{-1}$ , but an increase to 6.67 in the power of the peak at  $9.41 \text{ y}^{-1}$ .

We then modified our likelihood analysis to take account of the non-uniformity in data acquisition, dividing each bin into two parts (before and after the mean live time) with appropriate weightings. In contrast to the sensitivity of the Lomb-Scargle procedure to non-uniformity in the data acquisition process, we find the likelihood procedure to be quite insensitive to the non-uniformity represented by the Super-Kamiokande data. The “single boxcar” and “double boxcar” time window functions yield essentially the same power spectrum, that shown in

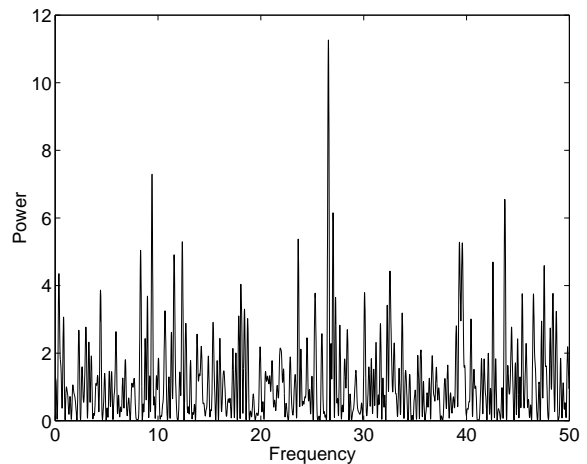


FIG. 6: Power Spectrum of Super-Kamiokande 10-day data computed by the likelihood method.

Figure 6, in which the peaks at  $26.55 \text{ y}^{-1}$  and at  $9.42 \text{ y}^{-1}$  still have  $S = 11.26$  and  $7.29$ , respectively. This again shows the superiority of the likelihood method over the Lomb procedure used, since the latter employed only the mean time, whereas the former utilized mean, start, and stop times, and more importantly, the measurement errors.

We previously noted [13] that  $9.41 \text{ y}^{-1}$  and  $26.57 \text{ y}^{-1}$  sum to  $35.98 \text{ y}^{-1}$ , which is the sampling frequency, from which we inferred that one peak is spurious, being an alias of the other. Since the peak at  $26.57 \text{ y}^{-1}$  had the bigger power, and since it falls in the band of twice the synodic rotation frequency, we assumed that the peak at  $9.41 \text{ y}^{-1}$  was merely an alias. However, when the Super-Kamiokande data were subdivided into 5-day bins [14], the peak at  $26.57 \text{ y}^{-1}$  disappeared, but the peak at  $9.41 \text{ y}^{-1}$  remained. Hence it is now clear that the peak at  $26.57 \text{ y}^{-1}$  was an alias of the peak at  $9.41 \text{ y}^{-1}$ , not the other way around.

We analyzed the new Super-Kamiokande 5-day data using the likelihood procedure, taking account of the experimental error estimates, the mean live time and the start and end time of each bin [34]. The resulting power spectrum is shown in Figure 7. The biggest peak, A, in the range 0– $100 \text{ y}^{-1}$  is that at  $9.43 \pm 0.05 \text{ y}^{-1}$ , which now has the enhanced power  $S = 11.51$ . In agreement with the analysis of the Super-Kamiokande group, we find that the peak at  $26.57 \text{ y}^{-1}$  has disappeared. Hence  $9.43 \text{ y}^{-1}$  is the primary peak, and the  $26.57 \text{ y}^{-1}$  peak was an alias in the 10-day data. Since the 5-day binning is also very regular, the power spectrum of the timing now has a huge peak at  $72.01 \text{ y}^{-1}$  (period 5.07 days), so an alias peak would be expected at  $72.01 - 9.43 = 62.58 \text{ y}^{-1}$ , and we do indeed find a peak (not shown in Fig. 7) at  $\nu = 62.56 \pm 0.08 \text{ y}^{-1}$  with  $S = 5.36$ . There are also notable peaks at  $39.28 \pm 0.05 \text{ y}^{-1}$  ( $S = 8.91$ ), labeled C, and  $43.72 \pm 0.06 \text{ y}^{-1}$  ( $S = 9.83$ ), labeled B in Fig. 7.

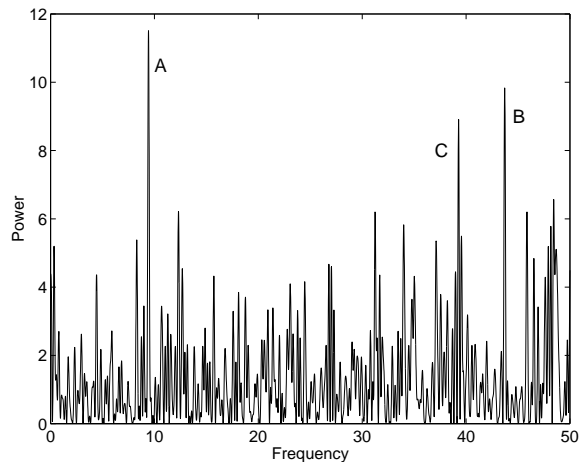


FIG. 7: Power Spectrum of Super-Kamiokande 5-day data computed by the likelihood method, taking account of measurement error, start time, and end time, of each bin.

The latter two peaks, plus that at  $9.43 \text{ y}^{-1}$ , are the three strongest peaks in the range  $0\text{--}100 \text{ y}^{-1}$ . The  $39 \text{ y}^{-1}$  and  $44 \text{ y}^{-1}$  peaks are much weaker in the 10-day data, presumably because the sampling time is too long.

#### EXPLANATION FOR THE PEAK FREQUENCIES

To understand these three peaks, it is helpful to seek guidance from measurements of the solar magnetic field. A power spectrum out to  $120 \text{ y}^{-1}$  of the photospheric field at Sun-center during the Super-Kamiokande data-acquisition interval is shown in Figure 8. We see that the fundamental and second harmonic of the rotation frequency are virtually absent, but there is a remarkable sequence of higher harmonics. By forming the combined spectrum statistic [9] of the third through the seventh harmonics, we obtain the estimate  $13.20 \pm 0.14 \text{ y}^{-1}$  for the synodic rotation frequency of the photospheric magnetic field, leading to the value  $14.20 \pm 0.14 \text{ y}^{-1}$  for the sidereal rotation frequency.

We see that peak C, at  $39.28 \text{ y}^{-1}$ , falls within the band of frequencies,  $39.60 \pm 0.42 \text{ y}^{-1}$ , of the third harmonic of the synodic rotation frequency of the magnetic field. We have applied the shuffle test [3, 35], randomly re-assigning flux and error measurements (kept together) to time bins. For this purpose, the shuffle test is more reliable than Monte Carlo simulations, since actual data are used. In this way we find that only 5 of 1,000 simulations yield a power larger than 8.91 (the power of peak C) in this search band. It appears, therefore, that peak C may be attributed to the effect of the Sun’s internal inhomogeneous magnetic field that necessarily rotates with the ambient medium. To check this assumption, we have determined the frequency for which the neutrino and magnetic data show the strongest correlation by means of the

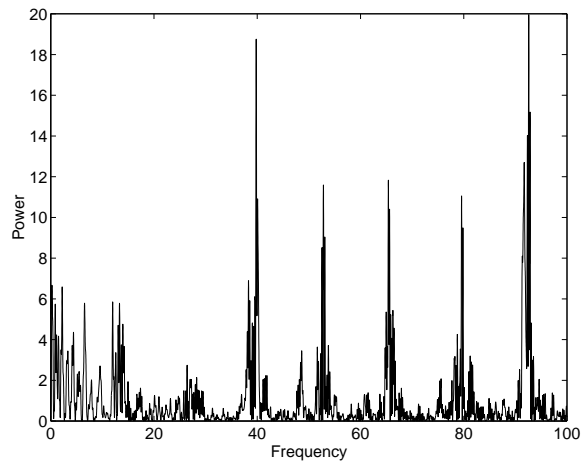


FIG. 8: Power spectrum of the disk-center solar magnetic field for the interval of operation of Super-Kamiokande.

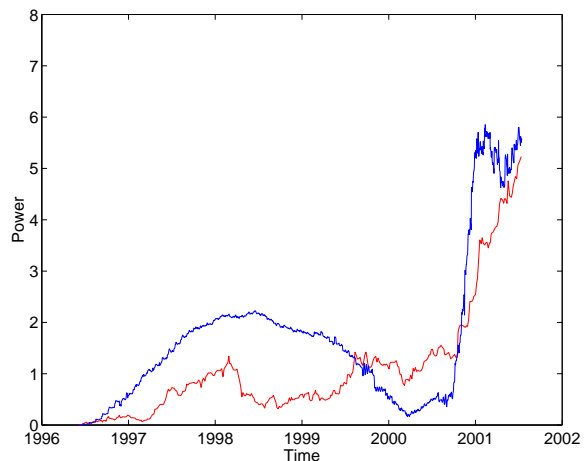


FIG. 9: Cumulative contribution to the final Rayleigh power of disk-center magnetic field (blue) and 5-day Super-Kamiokande data (red) for frequency  $39.56 \text{ y}^{-1}$ . The steep rise begins near solar maximum (2000.6).

joint spectrum statistic [9]. This frequency is found to be  $39.56 \text{ y}^{-1}$ . Figure 9 shows the cumulative Rayleigh powers derived from the neutrino and magnetic data for this frequency. We see that there is a remarkable correspondence, both powers growing from 1996 until 1998, then decreasing until about 2000.6 (solar maximum), after which both increase sharply, indicating again the influence of the solar cycle variations of magnetic structures in the convection zone.

We now consider peak A at  $9.43$  with power  $11.51$ , and peak B at  $43.72$  with power  $9.83$ . We presented evidence above for r-mode oscillations [29] in the Homestake and GALLEX-GNO data that appear to be the origin of the well-known Rieger oscillation [27] and of similar “Rieger-type” oscillations [28] that have been discovered in recent years. We therefore examine the possibility that peaks A

and B may be related to such oscillations interpreted as r modes.

R-modes are retrograde waves that, in a uniform and uniformly rotating model Sun, have frequencies

$$\nu(\ell, m, \text{syn}) = m(\nu_R - 1) - \frac{2m\nu_R}{\ell(\ell + 1)} \quad (2)$$

as seen from Earth, where  $\ell$  and  $m$  are two of the usual spherical-harmonic indices, and  $\nu_R$  is the sidereal rotation frequency (in cycles per year). If r-mode oscillations are to influence the solar neutrino flux, they must interfere with magnetic regions that co-rotate with the ambient medium. The interference frequencies will be given by

$$\nu = \left| m(\nu_R - 1) - \frac{2m\nu_R}{\ell(\ell + 1)} \pm m'(\nu_R - 1) \right| \quad (3)$$

where  $m'$ , the azimuthal index for the magnetic structure, may be different from that of the r-mode. For  $m' = m$ , equation (3) yields the frequency

$$\nu(\ell, m, \text{rot}) = \frac{2m\nu_R}{\ell(\ell + 1)}, \quad (4)$$

for the minus sign, and

$$\nu(\ell, m, \text{alias}) = 2m(\nu_R - 1) - \frac{2m\nu_R}{\ell(\ell + 1)} \quad (5)$$

for the plus sign. The frequencies given by (4) are the well-known Rieger-type frequencies. We may regard the frequencies given by (5) as aliases of these frequencies.

For  $\ell = 2$  and  $m = 2$  and for the range of values of  $\nu_R$  inferred from the magnetic-field data, equation (4) leads us to expect oscillations in the band  $9.47 \pm 0.09$ , and equation (5) leads us to expect oscillations in the band  $43.33 \pm 0.47$ . We see that the peaks A and B fall within these bands. On applying the shuffle test, we find only 2 cases out of 10,000 in which a peak with power larger than 11.51 occurs in the band  $9.47 \pm 0.09$ , and only 3 cases out of 1,000 that yield a power larger than 9.83 in the band  $43.33 \pm 0.47$ . Figure 10 shows the cumulative Rayleigh powers at these two frequencies as a function of time. These two frequencies not only have a very similar trend in their time evolution, but also some of the fine structure is even similar, indicating that they both originate in the same internal oscillation, an r-mode with  $\ell = 2$ ,  $m = 2$ . Note the contrast between Figs. 9 and 10, showing the different origins of the A and B peaks from that of C.

## PREDICTIONS AND CONCLUSIONS

While in the future an especially good test of these ideas will come from real-time data taken at low enough

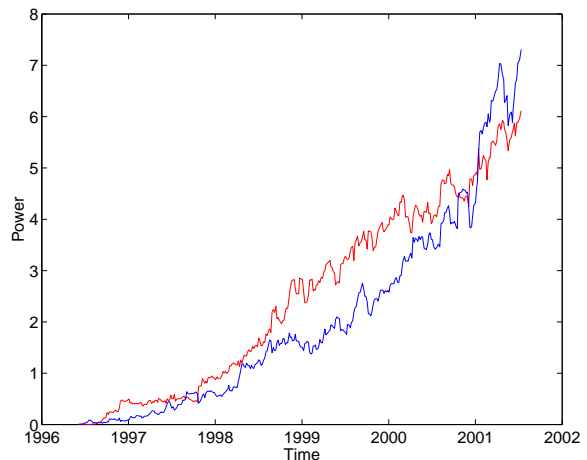


FIG. 10: Cumulative contribution to the final Rayleigh powers of oscillations at  $9.42 \text{ y}^{-1}$  (red) and  $43.72 \text{ y}^{-1}$  (blue).

energies to see the effect of the  $pp$  neutrino spectrum, a very interesting check should occur soon from SNO data. There has been a promise to use one-day bins, so the alias peak at  $62.56 \text{ y}^{-1}$  should not be seen. Figure 9 indicates that the  $39.3 \text{ y}^{-1}$  peak should be present, and that, with shorter sampling time, some of the higher harmonics of the magnetic field rotation may be observed also. Figure 10 indicates that the Rieger-type frequencies may also be present. Especially interesting could be a comparison of the amplitudes of the flux modulations for the charged-current and neutral-current interactions, since with spin change as well as flavor change responsible, in principle a difference in these two could indicate that the neutrinos are Majorana particles. If, however, the transitions are all to the sterile state, then the result could not distinguish Majorana from Dirac neutrinos.

The analysis of Super-Kamiokande data, when combined with the results of analyses of Cl and Ga data, yields a variety of evidence for variability of the solar neutrino flux. It should be stressed that this evidence can all be understood in terms of known fluid-dynamic and solar-dynamic processes in the standard solar model. In particular, the frequency peaks in the Super-Kamiokande data are all explained. These same peaks are seen in the analysis by the Super-Kamiokande collaboration, but their inappropriate analysis method makes these peaks appear insignificant, whereas our more sensitive method—using more of the experimental information—is needed to find these small modulations significantly [36]. Ref. [36] spells out in detail which aspects of the two analyses lead to the differences in sensitivity, but a simple summary is that the Super-Kamiokande analysis could claim a modulation only if it were greater than 10%, but the effect we detect significantly is at the 7% level. The result of all this evidence for solar neutrino flux variation, in view of KamLAND's input, is a subdominant RSFP process requiring new physics in the form of

a large transition magnetic moment and a light sterile neutrino.

### ACKNOWLEDGMENTS

We are indebted to G.M. Fuller, J.D. Scargle, G. Walther, M.S. Wheatland, and S.J. Yellin for assistance and helpful discussions. D.O.C. has been supported by a grant from the Department of Energy No. DE-FG03-91ER40618, and P.A.S. is supported by grant No. AST-0097128 from the National Science Foundation.

### APPENDIX: BRIEF EXPLANATION OF THE LIKELIHOOD CALCULATION

The log-likelihood that the data  $x_r$  may be fit by a given functional form  $X_r$  is given [34] by

$$L = -\frac{1}{2} \sum_{r=1}^R \frac{(x_r - X_r)^2}{\sigma_r^2}, \quad (1)$$

apart from a constant term, where  $r = 1, \dots, R$  enumerates the data bins. We adopt

$$x_r = \frac{g_r}{\text{mean}(g_r)} - 1, \quad (2)$$

where  $g_r$  are the flux measurements, and scale the error estimates accordingly. We adopt the functional form

$$X_r = \frac{1}{D_r} \int_{t_{sr}}^{t_{er}} dt (Ae^{i2\pi\nu t} + A^*e^{-i2\pi\nu t}), \quad (3)$$

where  $D_r$  is the duration of each bin. Then, for each frequency, we adjust the amplitude  $A$  to maximize the likelihood [3].

What is significant is not the actual log-likelihood as computed from (1), but the increase in the log-likelihood over the value that corresponds to a constant flux, which is given (apart from the same constant term) by

$$L_0 = -\frac{1}{2} \sum_{r=1}^R \frac{x_r^2}{\sigma_r^2}. \quad (4)$$

Hence the relative log-likelihood, which is equivalent to the power spectrum, is given by

$$S = L - L_0, \quad (5)$$

i.e., by

$$S = \frac{1}{2} \sum_{r=1}^R \frac{x_r^2}{\sigma_r^2} - \frac{1}{2} \sum_{r=1}^R \frac{(x_r - X_r)^2}{\sigma_r^2}. \quad (6)$$

Application of the formalism above to one frequency in the Super-Kamiokande data shows the magnitude of

the flux modulation. For  $\nu = 9.43$ , and for zero time chosen arbitrarily to be the date 1970.00, we find that  $A = 0.0192 - 0.0291i$ . This corresponds to a depth of modulation of the neutrino flux of 7%.

- 
- [1] K. Eguchi et al., *Phys. Rev. Lett.* **90**, 021802 (2003).
  - [2] C.-S. Lim and W.J. Marciano, *Phys. Rev. D* **37**, 1368 (1988); E.Kh. Akhmedov, *Sov. J. Nucl. Phys.* **48**, 382 (1988) and *Phys. Lett.* **B213**, 64 (1988).
  - [3] P.A. Sturrock, G. Walther and M.S. Wheatland, *Astrophys. J.* **491**, 409 (1997).
  - [4] P.A. Sturrock, G. Walther and M.S. Wheatland, *Astrophys. J.* **507**, 978 (1998).
  - [5] P.A. Sturrock, J.D. Scargle, G. Walther and M.S. Wheatland, *Astrophys. J.* **523**, L177 (1999).
  - [6] P.A. Sturrock and J.D. Scargle, *Astrophys. J.* **550**, L101 (2000).
  - [7] P.A. Sturrock and M.A. Weber, *Astrophys. J.* **565**, 1366 (2002).
  - [8] P.A. Sturrock and M.A. Weber, "Multi-Wavelength Observations of Coronal Structure and Dynamics—Yohkoh 10th Anniversary Meeting" (COSPAR Colloquia Series, P.C.H. Martens and D. Cauffman, eds., 2002), p. 323.
  - [9] P.A. Sturrock, astro-ph/0304148; hep-ph/0304106; P.A. Sturrock and M.S. Wheatland, astro-ph/0307353.
  - [10] B.C. Chauhan and J. Pulido, *JHEP* 0406, 008 (2004). The neutrino model used was suggested by one of us (D.O.C.) well after our paper was originally written, but delayed publication now enables us to utilize their excellent results.
  - [11] S. Fukuda et al., *Phys. Rev. Lett.* **86**, 5651 (2001).
  - [12] M.B. Smy, hep-ex/0206016 and <http://www-sk.icrr.u-tokyo.ac.jp/sk/lowe/index.html>
  - [13] P.A. Sturrock and D.O. Caldwell, *Bull. Am. Astron. Soc.* **34**, 1314 (2002); P.A. Sturrock, *Astrophys. J.* **594**, 1102 (2004). D.O. Caldwell and P.A. Sturrock, hep-ph/0305303; A. Milsztajn, hep-ph/0301252; M. Nakahata, <http://www-sk.icrr.u-tokyo.ac.jp/sk/lowe/frequencyanalysis/index.html>
  - [14] J. Yoo et al., *Phys. Rev. D* **68**, 092002 (2003).
  - [15] L. Wolfenstein, *Phys. Rev. D* **17**, 2369 (1978); *Phys. Rev. D* **20**, 2634 (1979); S.P. Mikheyev and A.Yu. Smirnov, *Sov. J. Nucl. Phys.* **42**, 913 (1985); *Nuovo Cimento* **9C**, 17 (1986).
  - [16] P.C. de Holanda and A.Yu. Smirnov, *Phys. Rev. D* **69**, 113002 (2004).
  - [17] B.T. Cleveland et al., *Astrophys. J.* **496**, 505 (1998).
  - [18] M.M. Guzzo and H. Nunokawa, *Astropart. Phys.* **12**, 87 (1999); J. Pulido and E.Kh. Akhmedov, *Astropart. Phys.* **13**, 227 (2000); E.Kh. Akhmedov and J. Pulido, *Phys. Lett.* **B485**, 178 (2000); O.G. Miranda, C. Peña-Garay, T.I. Rashba, V.B. Semikoz and J.W.F. Valle, *Nucl. Phys.* **B595**, 360 (2001) and *Phys. Lett.* **B521**, 299 (2001); J. Pulido, *Astropart. Phys.* **18**, 173 (2002).
  - [19] B.C. Chauhan and J. Pulido, *Phys. Rev. D* **66**, 053006 (2002) includes the SNO data in the fits.
  - [20] Q.R. Ahmad et al., *Phys. Rev. Lett.* **89**, 011301 and 011302 (2002).
  - [21] A. Aguilar et al., *Phys. Rev. D* **64**, 112007 (2001) and earlier references therein.

- [22] W. Hampel et al., *Phys. Lett.* **B447**, 127 (1999); M. Altmann et al., *Phys. Lett.* **B490**, 16 (2000).
- [23] J. Schou et al., *Astrophys. J.* **505**, 390 (1998).
- [24] S. Tsuneta et al., *Solar Phys.* **136**, 37 (1991).
- [25] E. Antonucci et al., *Astrophys. J.* **360**, 296 (1998).
- [26] T. Bai, *Bull. Am. Astron. Soc.* **34**, 953 (2002).
- [27] E. Rieger et al., *Nature* **312**, 623 (1984).
- [28] T. Bai, *Astrophys. J.* **388**, L69 (1992); *Solar Phys.* **150**, 385 (1994); J.N. Kile, and E.W. Cliver, *Astrophys. J.* **370**, 442 (1991).
- [29] J. Papaloizou, and J.E. Pringle, *Mon. Not. R. Astro. Soc.* **182**, 423 (1978); J. Provost, G. Berthomieu, and A. Rocca, *Astron. Astrophys.* **94**, 126 (1981); H. Saio, *Astrophys. J.* **256**, 717 (1982).
- [30] A. Friedland and A. Gruzinov, *Astropart. Phys.* **19**, 575 (2003).
- [31] L. Pandola, hep-ph/0406248.
- [32] P.A. Sturrock and D.O. Caldwell, hep-ph/0409064.
- [33] N. Lomb, *Astrophys. Space Sci.* **39**, 447 (1996); further developed by J.D. Scargle, *Astrophys. J.* **263**, 835 (1982); *Astrophys. J.* **343**, 874 (1989).
- [34] P.A. Sturrock, *Astrophys. J.* **594**, 1102 (2003); *ibid.* **605**, 568 (2004).
- [35] J.N. Bahcall and W.H. Press, *Astrophys. J.* **370**, 730 (1991).
- [36] P.A. Sturrock, D.O. Caldwell, J.D. Scargle, G. Walther, and M.S. Wheatland, hep-ph/0403246; P.A. Sturrock, hep-ph/0408017